Do Images of Biskyrmions Show Type-II Bubbles?

J. C. Loudon,[1,*] A. C. Twitchett-Harrison,[1] D. Cortés-Ortuño,[2] M. T. Birch,[3] L. A. Turnbull,[3] A. Štefančič,[4] F. Y. Ogrin,[5] E. Burgos-Parra,[5] N. Bukin,[5] A. Laurenson,[5] H. Popescu,[6] M. Beg,[2,7] O. Hovorka,[2] H. Fangohr,[7,2] P. A. Midgley,[1] G. Balakrishnan,[4] and P. D. Hatton[3]

[1] *Department of Materials Science and Metallurgy, University of Cambridge, 27 Charles Babbage Road, Cambridge, CB3 0FS, United Kingdom.*
[2] *Faculty of Engineering and Physical Sciences, University of Southampton, Southampton, SO17 1BJ, United Kingdom.*
[3] *Department of Physics, University of Durham, Durham, DH1 3LE, United Kingdom.*
[4] *Department of Physics, University of Warwick, Coventry, CV4 7AL, United Kingdom.*
[5] *School of Physics and Astronomy, University of Exeter, Exeter, EX4 4QL, United Kingdom.*
[6] *Synchrotron SOLEIL, Saint Aubin, BP 48, 91192 Gif-sur-Yvette, France.*
[7] *European XFEL GmbH, Holzkoppel 4, 22869 Schenefeld, Germany.*

(Dated: February 4, 2019)

Keywords: skyrmions, biskyrmions, magnetic bubbles, LTEM, x-ray holography.

The intense research effort investigating magnetic skyrmions and their applications for spintronics has yielded reports of more exotic objects including the biskyrmion, which consists of a bound pair of counter-rotating vortices of magnetization. Biskyrmions have been identified only from transmission electron micrographs and have not been observed by other techniques, nor seen in simulations carried out under realistic conditions. Here we combine quantitative Lorentz transmission electron microscopy (LTEM), x-ray holography and micromagnetic simulations to search for biskyrmions in MnNiGa, a material in which they have been reported. We find only type-I and type-II magnetic bubbles and demonstrate that images purported to show biskyrmions can be explained as type-II bubbles viewed at an angle to their axes. It is not the magnetization but the magnetic flux density resulting from this object that forms the counter-rotating vortices.

A magnetic skyrmion is a localized magnetic configuration with an integer, non-zero topological charge which can occur in magnetic materials [1]. The Bloch skyrmions considered here resemble magnetic vortices but have an integer topological charge rather than $\pm\frac{1}{2}$. The concept of a skyrmion was introduced in 1961 in the context of nuclear physics [2] and in 1989, magnetic skyrmions were predicted [3] to occur as a result of the competition between the Heisenberg exchange energy and the Dzyaloshinskii-Moriya interaction [4]. We use the term 'DM-skyrmions' to refer to such objects.

DM-skyrmions were found experimentally [5] in bulk MnSi in 2009. This prompted the recent intense research effort as magnetic skyrmions can be moved by electrical currents a million times smaller than those required to move ferromagnetic domain walls, making them promising objects for spintronic applications, notably racetrack computer memories [6–8]. The Dzyaloshinskii-Moriya interaction and hence DM-skyrmions can occur only in magnetic systems which lack an inversion symmetry due either to interfaces between different materials [9, 10] or because the crystal is non-centrosymmetric [5, 11, 12].

In contrast, magnetic bubbles can occur in centrosymmetric magnets and despite resembling DM-skyrmions, their origin is different [13, 14]. Magnetic bubbles can be generated in thin sheets of magnetic material where the easy axis is oriented out-of-plane. If the uniaxial magnetocrystalline anisotropy is sufficiently large, the magnetization points out of plane and striped magnetic domains form as shown by the micromagnetic simulation in the left-hand panel of Figure 1(a).

When a magnetic field is applied out-of-plane (H_z), domains with an antiparallel magnetization shrink until they break into roughly circular domains called magnetic bubbles as shown in Figure 1(a) (and in more detail in Video S1 and Figure S2, Supporting Information). Different sizes and densities of magnetic bubbles result from different field treatments and repeated field pulses can be used to create a dense hexagonal array of bubbles [13]. Magnetic bubbles of size 0.5 mm were likely first imaged in 1959 in oxides such as $YFeO_3$ using polarized light microscopy [15] and designs for a computer memory using bubbles a few microns in diameter were given in a 1967 review [16]. Much smaller bubbles around 100 nm in diameter have been produced in other materials as part of the recent research into magnetic skyrmions [17–20].

Two types of bubble can be distinguished in Figure 1(a) and are sketched in the right-hand panel. In a type-I bubble [21], the magnetization in the domain wall surrounding the bubble's core circulates either clockwise or anticlockwise with equal probability. This is different from skyrmions where the magnetic chirality is determined by the chirality of the crystal in bulk systems and the interfacial symmetry breaking in thin films. Like skyrmions, type-I bubbles have a topological charge of 1 and so are topologically non-trivial and are sometimes called 'skyrmion-' or 'skyrmionic-bubbles' [22–25]. In a type-II bubble (also called the 'onion state' –

* j.c.loudon@gmail.com

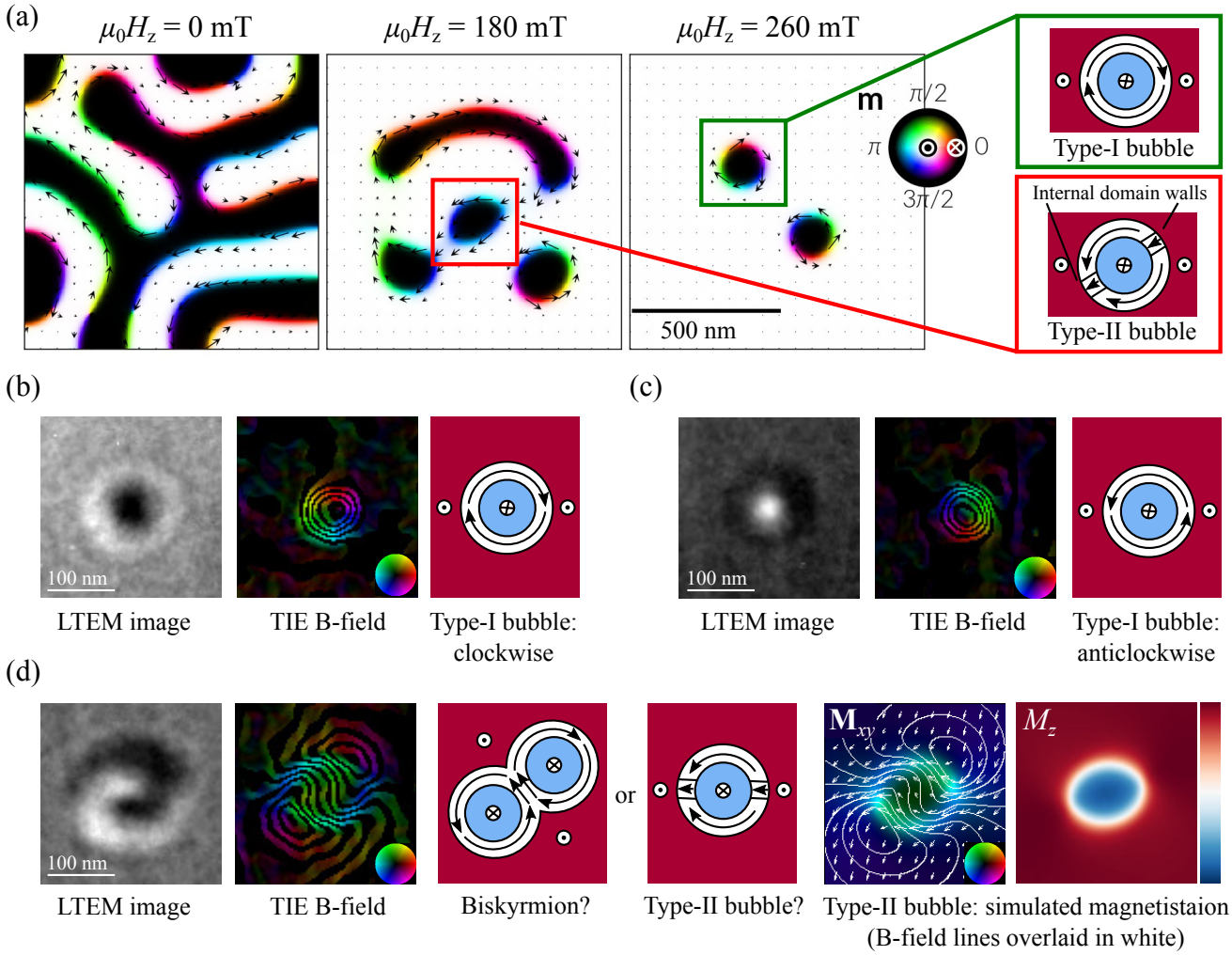

FIG. 1. (a) Micromagnetic simulations showing the formation of different types of magnetic bubble as the applied field H_z is increased. (b)-(d) Electron micrographs showing bubbles in MnNiGa together with the projected B-field reconstructed from a defocus series of such images and the magnetic states to which they correspond with arrows indicating the magnetization direction. Micrographs like (d) have been identified as biskyrmions but more likely show type-II bubbles. (See text for details.) The images were acquired at room temperature in an out-of-plane applied field of 233 mT at defocus $\Delta f = -1.41$ mm. The projected B-field lines correspond to the cosine of 100 times the phase of the exit wavefunction of the electron beam and their direction is indicated by the inset color wheels. The right-hand panel of (d) labeled $\mathbf{M}_{xy}$ shows a micromagnetic simulation of the projected magnetization normal to the electron beam of a type-II bubble viewed at 9.5° to its axis, indicated by arrows and colors. B-field lines are overlaid in white and closely resemble the TIE reconstruction. The final panel shows the projected magnetization component parallel to the beam, M_z, the strength indicated by the red-blue color bar with red denoting positive values, blue negative and white zero.

the name derives from a related structure in magnetic rings [23, 26]), the circulation sense of the magnetization reverses at points we term 'internal domain walls'. Our simulations show they have topological charge 0 in agreement with Ref. [23] making these magnetic structures topologically trivial.

The left hand panels of Figures 1(b) and (c) show electron micrographs of type-I bubbles in $Mn_{0.325}Ni_{0.324}Ga_{0.350}$ (subsequently referred to as MnNiGa) and it can be seen that they appear as a black circle for one circulation direction and white for the other at a given defocus. Electron micrographs are sensitive to the component of the magnetic flux density normal to the electron beam averaged through the sample thickness along the beam direction – a quantity we term the 'projected B-field'. The projected B-field can be recovered from a series of such images acquired at different defoci using the transport of intensity equation (TIE) [27] as shown in the central panels of (b) and (c). In a type-I bubble there is no stray field so the magnetization is proportional to the B-field and the bubble type and circulation sense are readily identified as shown in the right-hand panels.

In 2014, images with both black and white features

like that shown in the left panel of Figure 1(d) were reported in $La_{2-2x}Sr_{1+2x}Mn_2O_7$ ($x = 0.315$) [18] and the same state has been identified in $(Mn_{1-x}Ni_x)_{0.65}Ga_{0.35}$ ($x = 0.5$) [20] and amorphous Fe-Gd thin films with perpendicular magnetic anisotropy [19], none of which exhibit the Dzyaloshinskii-Moriya interaction. These images were identified as showing biskyrmions because the projected B-field reconstructed from such images showed two counter rotating vortices as seen in Figure 1(d).

No mathematical model has been proposed for a biskyrmion but it consists of two cores (regions where the magnetization opposes the applied field) shown in blue in the sketch in Figure 1(d), surrounded by counter-rotating vortices. Images identified as showing biskyrmions range in appearance from black and white semi-circles to the interlocking black-white contrast of Figure 1(d) sometimes called 'Yin-Yang' [23]. Yin-Yang contrast can be seen in images from $La_{1.37}Sr_{1.63}Mn_2O_7$ (Figure 2(c) of Ref. [18]) and MnNiGa (Figures 2(a) and 3 of Ref. [28]).

In this paper, we acquired images of magnetic bubbles from MnNiGa using x-ray holography with extended references [29, 30] and Lorentz transmission electron microscopy and compared these with simulations. The right two panels of Figure 1(d) show a micromagnetic simulation of a type-II bubble when viewed at an angle to its axis with the projected B-field shown by white lines. Even though the simulated bubble has a single core as seen in M_z, the B-field has two counter-rotating vortices and closely resembles the B-field derived from experimental images. Thus we show that the counter-rotating vortices in the B-field need not correspond to similar vortices in the magnetization and the object identified as a biskyrmion is more likely a conventional type-II bubble viewed at an angle to its axis.

Only a few studies have reported generating biskyrmions in computer simulations such as Refs. [31] and [32] which are based on a Heisenberg-like spin model. The former paper deals only with thin samples using reduced parameters whereas the latter considers frustrated exchange interactions. We chose to use micromagnetic simulations as they are best suited to the length scales relevant to our experiments. We could not find a biskyrmion state by varying the material parameters within the range estimated from experiments, irrespective of whether there was a Dzyaloshinskii-Moriya interaction, and observed only type-I and type-II bubbles.

To search for biskyrmions experimentally, we acquired x-ray holograms which give the out-of-plane component of the magnetization averaged through the sample thickness (Section S3, Supporting Information). The MnNiGa sample used was a 200 nm thick, 10×5 μm single crystal plate with its large surfaces normal to the [001] magnetic easy axis. It was cut from a single grain of a polycrystal using a focused ion-beam microscope and the sample used for transmission electron microscopy was cut from the same grain (Sections S2–S4, Supporting Information). MnNiGa has a hexagonal crystal structure with space group $P6_3/mmc$ and lattice parameters $a = b = 4.15$ Å and $c = 5.33$ Å (Section S1, Supporting Information).

The sample was viewed in [001] and a field sweep from 0 to 284 mT was first carried out at room temperature with the field applied normal to the sample's surface. At low field, stripe domains were observed. As the field was increased, those domains opposed to the field first narrowed and then fragmented above 250 mT to become a sparse array of single-cored bubbles each with an average diameter of 120 nm separated by 650 nm. This process of bubble formation closely resembled the micromagnetic simulations in Figure 1.

The sample was then heated above its Curie temperature of 350 K and cooled back to room temperature in a field of 35 mT which produced a dense array of bubbles. The field was then swept from 0 to 400 mT and Figure 2(a) shows images acquired during this procedure. It can be seen from Figures 2(a) and (b) that the bubbles shrank to about half their original size as the field was increased although their spacing remained constant to within the margin of error. At no point was there any indication of magnetic features with the double core that would be expected from a biskyrmion.

It is difficult to distinguish type-I and II bubbles from an x-ray hologram as the out-of-plane magnetization is very similar in both cases but the linescans in Figure 2(c) indicate that these are likely to be type-II bubbles. Scanning in one direction, the magnetization reverses between the bubbles and can be fit with the expected hyperbolic tangent profile [33] with a domain wall width of 47 ± 5 nm. Scanning in the other direction, the magnetization does not fully reverse as indicated by the white haze between the bubbles in Figure 2(a) implying an in-plane component of the magnetization persists between the bubbles. The micromagnetic simulation in Figure 1(a) for 180 mT shows this happens near the internal domain walls of closely-spaced type-II bubbles.

To obtain experimental information on the in-plane component of the magnetization, Lorentz transmission electron micrographs were acquired. Such images are not sensitive to the magnetization itself but to the projected B-field. The sample was a single crystal MnNiGa lamella thinned on the (001) plane to two different thicknesses: 110–180 nm and in the thinner region and 200–230 nm in the thicker (Section S6 and Figure S5, Supporting Information).

Again, the process by which bubbles formed closely resembled the predictions of the micromagnetic simulations shown in Figure 1(a). Only striped domains were observed at room temperature when an initial field of 143 mT was applied normal to the lamella. When the field was increased to 233 mT, coexisting bubbles and striped domains were observed as shown in Figure 3(a), taken from the thicker region of the sample. All the electron micrographs in this paper have the same orientation indicated by the crystallographic directions in square brackets. The black-white contrast indicated the bubbles were the same object previously identified as a biskyrmion. Figure S5, Supporting Information shows

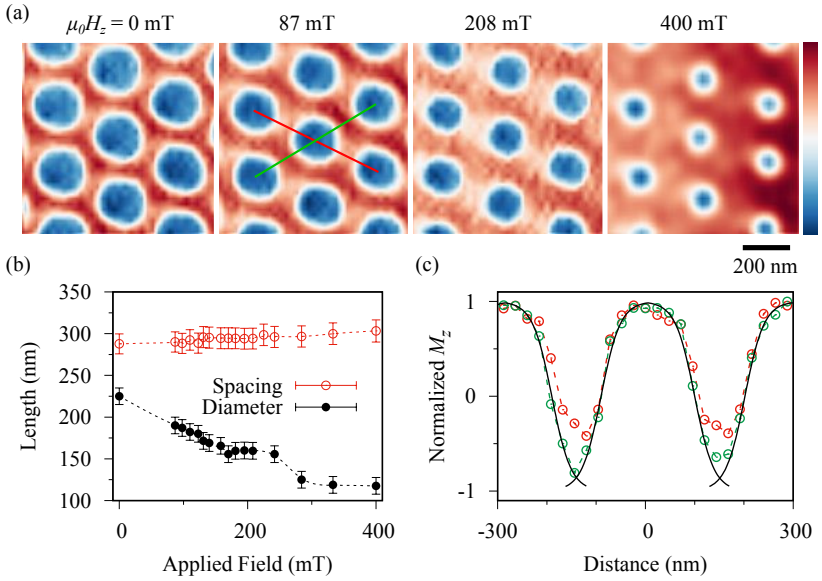

FIG. 2. (a) X-ray holograms showing the component of the magnetization normal to the specimen (M_z) at room temperature as the field applied normal to the specimen plane is increased. The strength of M_z is indicated by the color bar with red denoting positive values, blue negative and white zero. (b) The effect of increasing the applied field on the average center-to-center spacing of the bubbles and their diameter. (c) Linescans taken in the directions shown in (a) by the red and green lines. Solid black lines indicate hyperbolic tangent fits to the magnetic domain walls (see text).

that the same state also occurred in the thinner region even though the diameter of the bubbles was 40% less and their spacing 30% less than those in the thicker region.

Ten such images were acquired under the same conditions, each with a different defocus and the transport of intensity equation [27] was used to calculate the projected B-field, resulting in Figure 3(b). It can be seen that each bubble has the two counter-rotating vortices characteristic of a 'biskyrmion'. As the sample thickness and defocus had been measured (Section S4, Supporting Information), the B-field was obtained quantitatively and in absolute units.

The projected B-field was used as an inspiration to create an analytic model for the magnetization. The model is described in Section S7, Supporting Information and represents the magnetization averaged through the thickness of the sample in the electron beam direction. It consists of a modified type-II bubble in which the component of the magnetization normal to the electron beam does not follow the domain wall surrounding the bubble but is inclined to it as shown in Figure 3(f). The likelihood of such a bubble occurring is discussed later but for now it serves to show that the data can be explained by a bubble with a single core without the need to invoke a biskyrmion.

Defocused images were simulated using this model as described in the Section S7, Supporting Information. The parameters of the model such as the saturation magnetization, domain wall width and angle at which the magnetization was inclined to the wall were varied using a simplex algorithm [34] to minimize the normalized mean square difference between the experimental and simulated images (χ^2). Figure 3(c) shows the results of this for one of the bubbles.

Usually χ^2 close to 1 indicates a good fit but since the images showed additional contrast from slight thickness undulations due to ion milling, regions showing no magnetic contrast were used to establish that χ^2 between 2 and 3 indicated a good fit. Our fit gave $\chi^2 = 6.3$ and it can be seen from the difference images in Figure 3(c) that the fit is close but not perfect. It nevertheless reproduces all the features of the images.

The projected B-field calculated from the defocus series using the transport of intensity equation is shown in Figure 3(d) and it can be seen that it closely resembles the B-field calculated from the analytic model of the magnetization shown in (e). The magnetization itself is shown in (f) and it can be seen that it is has a single core rather than the double core required for a biskyrmion.

The fitting procedure was repeated for 19 bubbles in the same defocus series yielding a saturation magnetization $\mu_0 M_s = 0.0551 \pm 0.0006$ T and a domain wall width of $\delta = 47 \pm 1$ nm which is in good agreement with the value of 47 ± 5 nm derived from x-ray holography. The average values of the other parameters used in the model are listed in Table S1, Supporting Information.

We also found that different types of bubble can coexist and transitions between them can be stimulated by abruptly tilting the sample by 1° in an out-of-plane field of 233 mT. We acquired videos of these transitions and found that after tilting, most bubbles retained their original state but a few changed their state for up to a minute after tilting with each bubble changing faster than the frame rate of 1.15 s. The different transitions are shown

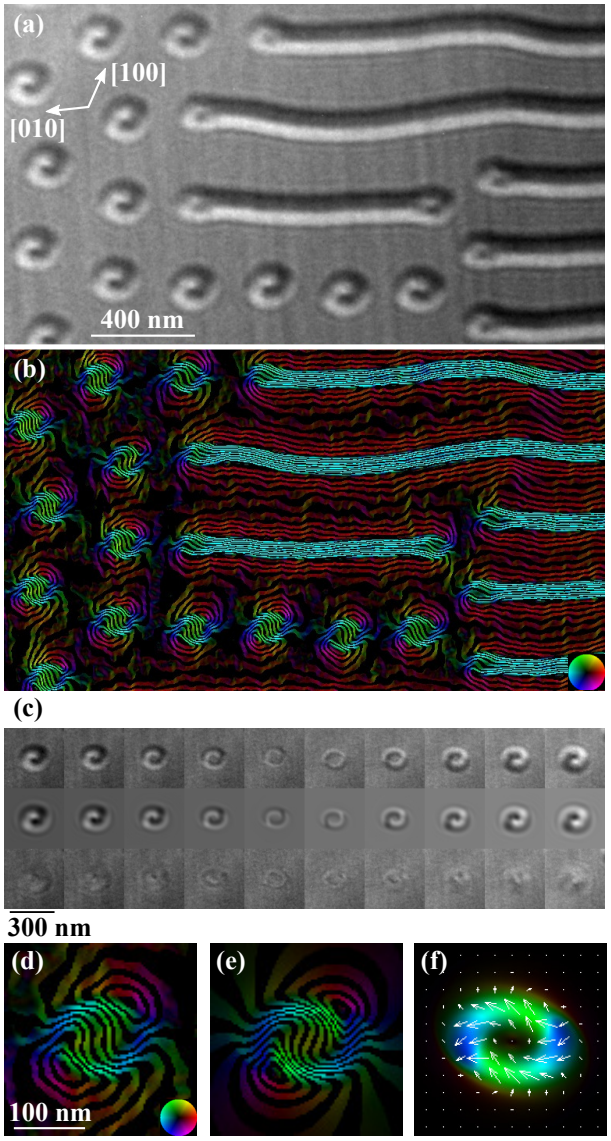

FIG. 3. (a) Electron micrograph showing striped domains and bubbles in MnNiGa at room temperature in an out-of-plane applied field of 233 mT with defocus $\Delta f = -1.410$ mm. (b) Projected B-field calculated from a defocus series of such images. The color wheel shows the direction of the field and the field lines correspond to the cosine of 100 times the phase of the exit wavefunction of the electron beam. (c) Top row: experimental defocus series of one bubble taken at defoci $\Delta f = -1.410$, -1.128, -0.846, -0.564, -0.282, 0.282, 0.564, 0.846, 1.128, 1.410 mm (left to right). Middle row: simulated defocus series. Bottom row: difference between experimental and simulated images. (d) Projected B-field for this bubble calculated from the defocus series and (e) from the simulated bubble. (f) Simulated projected magnetization from which (e) was calculated.

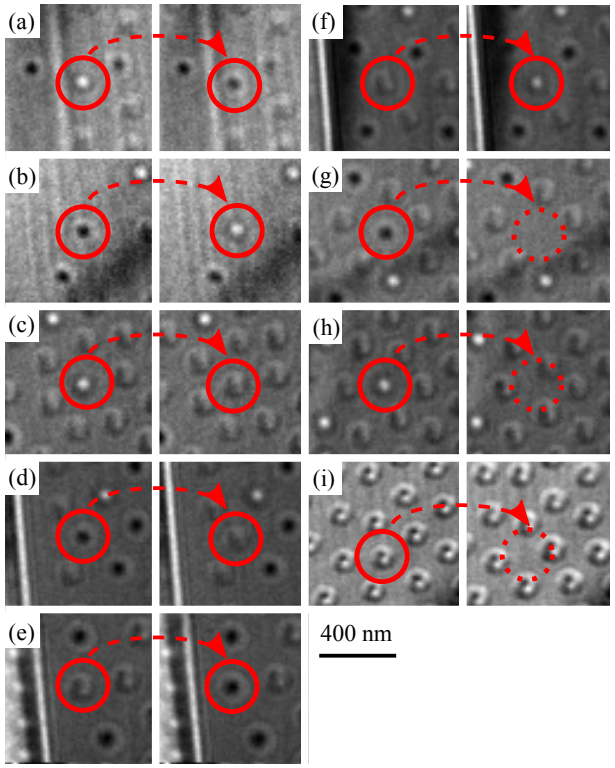

FIG. 4. Transformations of bubbles in MnNiGa (see text). The transitions occurred after a sudden tilt of 1° in an out-of-plane field of 233 mT and the right-hand images were acquired 1.15 s after the left-hand ones at $\Delta f = 1.682$ mm as part of a video. Unlike the other images, those in (i) were acquired incidentally as part of a defocus series. The two images were taken 15 s apart with the left at $\Delta f = 0.846$ and the right at $\Delta f = 1.128$ mm.

in Figure 4. We observed type-I bubbles reversing their helicity (Figure 4(a) and (b)); type-I bubbles of either helicity transforming into bubbles exhibiting 'biskyrmion' contrast ((c) and (d)) and *vice-versa* ((e) and (f)) as well as type-I bubbles and 'biskyrmions' transforming into the spin-aligned state and so vanishing from the image ((g), (h) and (i)).

As we argue, the 'biskyrmions' are most likely type-II bubbles. Yu *et al.* [17] have shown that transitions between type-I and type-II bubbles occur this way in their electron microscopy study of magnetic bubbles in $BaFe_{12-x-0.05}Sc_xMg_{0.05}O_{19}$, $x = 0.16$. They found that transitions between type-I and II bubbles can be stimulated by tilting the sample 1.5° in a vertical field of 80 mT. Like us, they also find that bubbles form by the fragmentation of stripe domains and that bubbles of both type and helicity can coexist.

We have shown that images purported to show biskyrmions can be explained by the analytic model described in Section S7, Supporting Information in which a type-II bubble with a single core is modified so that the magnetization does not follow the domain wall surrounding the bubble but is inclined to it. We now discuss whether such a magnetic structure is plausible.

To make this assessment, we performed micromagnetic simulations described in the Section S5, Supporting Information. First we randomly initialized the magnetic

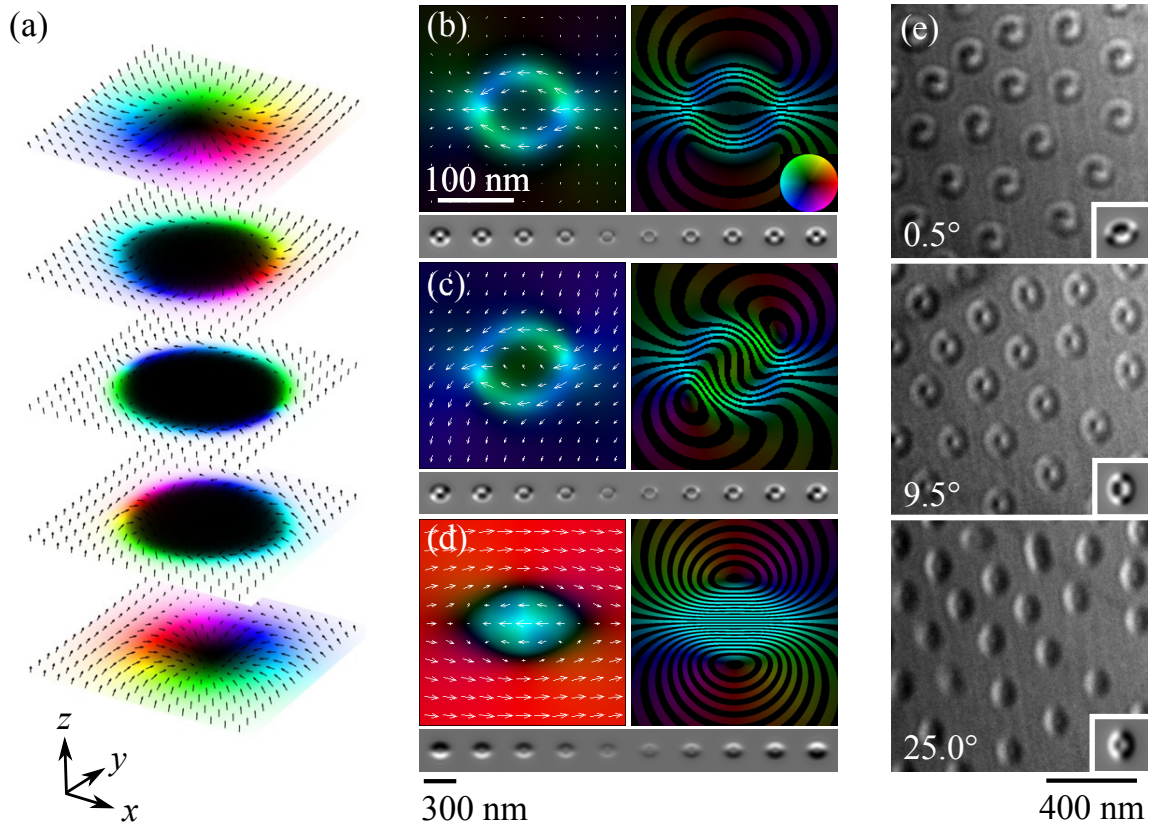

FIG. 5. (a) Magnetization of a simulated type-II bubble displayed in 3 dimensions as equally spaced slices. The sample surfaces lie in the xy plane and the line joining the internal domain walls is parallel to x. The uniaxial magnetocrystalline anisotropy and applied field are parallel to z. (b) Projected magnetization $\mathbf{M}_{xy}$ (left) and B-field (right) for the electron beam parallel to the bubble's axis z with a defocus series for these conditions shown beneath. (c) Projected magnetization and B-field for a sample tilted 9.0° about x and 3.5° about y with respect to the electron beam. The same simulation is shown in Figure 1(d). The associated defocus series is shown beneath. (d) Projected magnetization and B-field for a sample tilted 25° about y. Its defocus series is shown beneath. The simulated defocus series have the same defoci as those in Figure 3. (e) Electron micrographs of magnetic bubbles acquired with an out-of-plane applied field of 201 mT with defocus $\Delta f = 0.872$ mm at room temperature. Each image shows the same array of bubbles as the specimen is tilted about a horizontal axis by the angles given in the bottom left. Inserts at the bottom right show simulated images for tilt angles -9, 0 and 16°.

configuration and performed the field sweep shown in Figure 1(a) and Video S1. This produced only conventional type-I and type-II bubbles. We then seeded the simulation with a type-II bubble and the structure relaxed to give a conventional type-II bubble. When seeded with the modified type-II structure, the structure proved unstable and turned into the saturated state. Thus it is likely that the modified type-II bubble does not represent the true structure of the bubble but is the result of averaging the 3 dimensional structure through the sample thickness.

The 3 dimensional structure of a type-II bubble produced by micromagnetic simulations is shown in Figure 5(a) and it can be seen that it varies considerably throughout the thickness of the specimen. The wall surrounding the bubble is type-II near the center but near the surfaces the magnetization points radially. This was observed in simulations of samples from 80–200 nm thickness (Figure S4, Supporting Information) and is a well-known effect caused by the magnetization near the surface aligning with the stray field [35–37]. It was predicted in 1973 and soon could be confirmed experimentally using the new techniques of x-ray and electron magnetic tomography which are being developed to map magnetic structures in 3 dimensions [38, 39].

If the bubble's magnetization is averaged through the specimen thickness along its axis, the contributions above and below the central plane cancel and the bubble appears as a conventional type-II bubble as shown in Figure 5(b) with the corresponding defocus series shown below. There is no guarantee, however, that the electron beam will be parallel to the bubble's axis and so we investigated the appearance of such a structure if projected at an angle to its axis.

It proved difficult to recreate the same size of bubble as that seen experimentally as the bubble's size depends on the interaction with neighboring bubbles, the sample edges and pinning sites. Experimentally, we found that

the magnetic states that occurred were history dependent. For example, the bubbles in Figure 3 had an average diameter of 117 nm. After the sample was tilted to 32° and back to 0° maintaining a field of 233 mT parallel to the electron beam, the average diameter was 75 nm.

We could simulate isolated bubbles of diameter 120 nm, close to the observed diameter of 117 nm, in 100 nm thick samples. Simulations close to the experimental thickness of 200 nm produced bubbles at least double the radius although they had the same structure (Figure S4, Supporting Information). As the appearance of the images depends crucially on the size of the bubble, we used the simulations for 100 nm thickness and renormalized the thickness and saturation magnetization to match the experimental values to calculate the appearance of the electron micrographs. The tilting angles we quote here are scaled to match a 200 nm thickness.

The effect of tilting the specimen 9.0° about x and 3.5° about y is simulated in Figure 5(c) and it can be seen that the projected B-field closely resembles that derived from experimental measurements shown in Figure 3 as does the simulated defocus series below. A higher tilt angle of 25° with respect to y (Figure 5(d)) produced the half-white half-black appearance of the images identified as biskymrions in Refs. [18–20, 40–42].

To confirm these predictions, we acquired images of the magnetic bubbles shown in Figure 5(e) and it can be seen that their appearance changed profoundly with the tilt angle. When the specimen plane was nearly normal to the electron beam (0.5°), the bubbles had the Yin-Yang appearance discussed earlier. At 9.5°, the images resembled the simulations with the electron beam parallel to the axis of the bubble. At 25.0°, the images appeared half-white half-black.

Simulations of these images are shown as insets and it can be seen that there is a close resemblance. The relative tilt angles between the simulated images are in good agreement with those measured experimentally. There is a 9° offset in the absolute angle which may be because the sample's surface is not quite normal to the easy axis as would be typical for this type of specimen preparation. We estimated this offset to be around 7° from the tilt required to reach the [001] easy axis from the specimen's initial position in the microscope. Given the hysteresis in the magnetic configurations discussed earlier, it is also possible that the axes of the bubbles can become pinned so their tilting angles do not correspond to the specimen tilt.

Thus we conclude that there is no need to invoke a new magnetic state to explain the appearance of the images previously identified as biskyrmions. Such images, whether Yin-Yang in appearance like those in Figure 2(c) of Ref. [18] and Figures 2(a) and 3 of Ref. [28] or half-black half-white as seen in Refs. [18–20, 40, 41] can be explained as conventional type-II bubbles with topological charge 0, viewed at an angle to their symmetry axes. Similar conclusions were reached in a recent preprint [43] although the authors do not make a direct comparison between simulated and experimental images.

ACKNOWLEDGMENTS

This work was funded by the UK Skyrmion Project, EPSRC Programme Grant (EP/N032128/1) and the OpenDreamKit Horizon 2020 European Research Infrastructures project (#676541). X-ray holography was carried out using the COMET instrument [44] at the SEXTANS Beamline, Synchrotron SOLEIL, proposal ID: 20170252. All the data from the micromagnetic simulations performed in this study can be reproduced from the repository given in Ref. [45].

[1] Y. Dai, H. Wang, Z. Zhang, in *Skyrmions: Topological Structures, Properties and Applications*, (Eds: J. P. Liu, Z. Zhang, G. Zhao), CRC Press, Boca Raton, USA **2017**, pp. 1–32.
[2] T. H. R. Skyrme. *Nuc. Phys.* **1961**, *31* 556.
[3] A. N. Bogdanov, A. D. Yablonsky. *Sov. Phys. JETP* **1989**, *68* 101.
[4] I. E. Dzyaloshinskii. *Sov. Phys. JETP* **1964**, *19* 960.
[5] S. Mühlbauer, B. Binz, F. Jonietz, C. Pfleiderer, A. Rosch, A. Neubauer, R. Georgii, P. Böni. *Science* **2009**, *323* 915.
[6] N. S. Kiselev, A. N. Bogdanov, R. Schäfer, U. K. Rößler. *J. Phys. D: Appl. Phys.* **2011**, *44* 392001.
[7] A. Fert, V. Cros, J. Sampaio. *Nature Nanotechnology* **2013**, *8* 152.
[8] S. Parkin, S.-H. Yang. *Nature Nanotechnology* **2015**, *10* 195.
[9] T. Moriya. *Phys. Rev.* **1960**, *120* 91.
[10] W. Jiang, G. Chen, K. Liu, J. Zang, S. G. E. te Velthuis, A. Hoffmann. *Phys. Rep.* **2017**, *704* 1.
[11] A. Fert, P. M. Levy. *Phys. Rev. Lett.* **1980**, *44* 1538.
[12] A. Crépieux, C. Lacroix. *J. Magn. Magn. Mater.* **1998**, *182* 341.
[13] T. H. O'Dell. *Magnetic Bubbles*. Macmillan Press Ltd., London, UK **1974**.
[14] A. B. Bogatyrëv, K. L. Metlov. *ArXiv e-prints* **2017**.
[15] R. C. Sherwood. *J. Appl. Phys.* **1959**, *30* 217.
[16] A. H. Bobeck. *Bell Syst. Tech. J.* **1967**, *46* 1901.
[17] X. Z. Yu, M. Mostovoy, Y. Tokunaga, W. Zhang, K. Kimoto, Y. Matsui, Y. Kaneko, N. Nagaosa, Y. Tokura. *Nature Comm.* **2012**, *3* 988.
[18] X. Z. Yu, Y. Tokunaga, Y. Kaneko, W. Z. Zhang, K. Kimoto, Y. Matsui, Y. Taguchi, Y. Tokura. *Nature Communications* **2014**, *5* 3198.
[19] J. C. T. Lee, J. J. Chess, S. A. Montoya, X. Shi, N. Tamura, S. K. Mishra, P. Fischer, B. J. McMorran, S. K. Sinha, E. E. Fullerton, S. D. Kevan, S. Roy. *Appl. Phys. Lett.* **2016**, *109* 022402.

[20] W. Wang, Y. Zhang, G. Xu, L. Peng, B. Ding, Y. Wang, Z. Hou, X. Zhang, X. Li, E. Liu, S. Wang, J. Cai, F. Wang, J. Li, F. Hu, G. Wu, B. Shen, X.-X. Zhang. *Adv. Mater.* **2016**, *28* 6887.

[21] D. Morikawa, X. Z. Yu, Y. Kaneko, Y. Tokunaga, T. Nagai, K. Kimoto, T. Arima, Y. Tokura. *Appl. Phys. Lett.* **2015**, *107* 212401.

[22] I. Makhfudz, B. Krüger, O. Tchernyshyov. *Phys. Rev. Lett.* **2012**, *109* 217201.

[23] C. Phatak, O. Heinonen, M. D. Graef, A. Petford-Long. *Nano. Lett.* **2016**, *16* 4141.

[24] X. Z. Yu, Y. Tokunaga, Y. Taguchi, Y. Tokura. *Adv. Mater.* **2017**, *29* 1603958.

[25] F. Büttner, C. Moutafis, M. Schneider, B. Krüger, C. M. Günther, J. Geilhufe, C. v. Korff Schmising, J. Mohanty, B. Frau, S. Schaffert, A. Bisig, M. Foerster, T. Schultz, C. A. F. Vaz, J. H. Franken, H. J. M. Swagten, M. Kläui, S. Eisebitt. *Nature Physics* **2015**, *11* 225.

[26] J. Rothman, M. Kläui, L. Lopez-Diaz, C. A. F. Vaz, A. Bleloch, J. A. C. Bland, Z. Cui, R. Speaks. *Phys. Rev. Lett.* **2001**, *86* 1098.

[27] M. Beleggia, M. A. Schofield, V. V. Volkov, Y. Zhu. *Ultramicroscopy* **2004**, *102* 37.

[28] L. Peng, Y. Zhang, M. He, B. Ding, W. Wang, J. Li, J. Cai, S. Wang, G. Wu, B. Shen. *J. Phys.: Condens. Matter* **2018**, *30* 065803.

[29] T. A. Duckworth, F. Ogrin, S. S. Dhesi, S. Langridge, A. Whiteside, T. Moore, G. Beutier, G. van der Laan. *Optics Express* **2011**, *19* 16223.

[30] N. Bukin, C. McKeever, E. Burgos-Parra, P. S. Keatley, R. J. Hicken, F. Y. Ogrin, G. Beutier, M. Dupraz, H. Popescu, N. Jaouen, F. Yakhou-Harris, S. A. Cavill, G. van der Laan. *Scientific Reports* **2016**, *6* 36307.

[31] D. A. Garanin, E. M. Chudnovsky, X. Zhang. *Europhysics Letters* **2017**, *120* 17005.

[32] X. Zhang, J. Xia, Y. Zhou, H. Zhang, M. Ezawa. *Nature Communications* **2017**, *8*, 1 1717.

[33] J. M. D. Coey. *Magnetism and Magnetic Materials*. Cambridge University Press, Cambridge, UK **2010**.

[34] W. H. Press, B. P. Flannery, S. A. Teukolsky, T. T. Vetterling. *Numerical Recipes*. Cambridge University Press, Cambridge, UK **1992**.

[35] A. Hubert, R. Schäfer. *Magnetic Domains: The Analysis of Magnetic Microstructures*. Springer-Verlag, Berlin, Germany **2000**.

[36] J. C. Slonczewski. *J. Appl. Phys.* **1973**, *44* 1759.

[37] E. Schlömann. *J. Appl. Phys.* **1973**, *44* 1837.

[38] D. Wolf, L. A. Rodriguez, A. Béché, E. Javon, L. Serrano, C. Magen, C. Gatel, A. Lubk, H. Lichte, S. Bals, G. van Tendeloo, A. Fernández-Pacheco, J. M. de Teresa, E. Snoeck. *Chem. Mater.* **2015**, *27* 6771.

[39] C. Donnelly, M. Guizar-Sicairos, V. Scagnoli, S. Gliga, M. Holler, J. Raabe, L. J. Heyderman. *Nature* **2017**, *547* 328.

[40] L. Peng, Y. Zhang, M. He, B. Ding, W. Wang, H. Tian, J. Li, S. Wang, J. Cai, G. Wu, J. P. Liu, M. J. Kramer, A. Shen. *NPJ Quantum Materials* **2017**, *2* 30.

[41] L. Peng, Y. Zhang, W. Wang, M. He, L. Li, B. Ding, J. Li, Y. Sun, X.-G. Zhang, J. Cai, S. Wang, G. Wu, B. Shen. *Nano. Lett.* **2017**, *17* 7075.

[42] B. Ding, H. Li, X. Li, Y. Wang, Z. Hou, G. Xu, E. Liu, G. Wu, F. Wang, W. Wang. *APL Materials* **2018**, *6* 076101.

[43] Y. Yao, B. Ding, J. Cui, X. Shen, Y. Wang, R. Yu. *arXiv e-prints* **2018**, arXiv:1812.07332.

[44] H. Popescu, J. Perron, B. Pilette, R. Vacheresse, V. Pinty, R. Gaudemer, M. Sacchi, R. Delaunay, F. Fortuna, K. Medjoubi, K. Desjardins, J. Luning, N. Jaouen. *J. Synchrotron Rad.* **2019**, *26* 280.

[45] D. Cortés-Ortuño, J. C. Loudon, M. Beg, O. Hovorka, H. Fangohr. Supplementary data for: Do Images of Biskyrmions Show Type-II Bubbles? Zenodo doi:10.5281/zenodo.1420447. `Github:https://github.com/davidcortesortuno/paper_biskyrmions_bubbles`, **2019**.